Li_4SnS_4: Simulations of Its Structure and Electrolyte Properties

N. A. W. Holzwarth
Department of Physics, Wake Forest University, Winston-Salem, NC 27109, USA

First principles simulations show that the ground state crystal structure of Li_4SnS_4 is isomorphous to Li_4GeS_4, in agreement with experiment, and having interstitial sites in void channels along the c-axis. The simulations also show that a slightly meta-stable structure ($Li_4SnS_4^*$) is formed by moving Li ions from their central sites to the interstitial positions, consistent with X-ray patterns resulting from relatively low temperature synthesis methods. The simulations suggest that the $Li_4SnS_4^*$ material has favorable ion conducting properties.

I. Introduction

Recently, there has been significant progress in developing stable solid electrolytes with high ionic conductivity [1] which has been identified as a significant key to improved battery technologies. [2] Recent literature [3, 4, 5, 6] reports the use of Li_4SnS_4 and its alloys as a relatively stable solid electrolyte for use in all-solid-state Li batteries. Using first principles methods, we have examined structural properties of Li_4SnS_4, showing that it is likely to have two different crystal forms. We also present preliminary results on Li ion migration mechanisms in both crystal forms.

II. Computational methods

The computational methods used in this work are based on density functional theory (DFT), [7, 8] using the projected augmented wave (PAW) [9] formalism. The PAW basis and projector functions were generated by the ATOMPAW [10] code and the crystalline materials were modeled using the QUANTUM ESPRESSO [11] and ABINIT [12] packages. Visualizations were constructed using the *XCrySDEN*, [13, 14] *VESTA* [15] software packages.

The exchange correlation function is approximated using the local-density approximation (LDA). [16] The choice of LDA functional was made based on previous investigations [17, 18, 19] of similar materials which showed that provided that the lattice constants are scaled by a correction factor or 1.02, the simulations are in good agreement with experiment, especially lattice vibrational frequencies and heats of formation.

Calculations were performed with plane wave expansions of the wave function including $|\mathbf{k}+\mathbf{G}|^{\mathbf{2}} \leq 64$ bohr^{-2} and with a Brillouin-zone sampling grid of $4 \times 8 \times 8$ for the conventional unit cell. The partial densities of states were calculated as described in previous work, [20, 19] using weighting factors based on the charge within the augmentation spheres of each atom with radii $r_c^{\rm Li} = 1.6$, $r_c^{\rm Sn} = 2.3$, and $r_c^{\rm S} = 1.7$ in bohr units. The reported partial densities of states curves $< N^a(E) >$ were averaged over the atomic sites of each type a.

Simulation of Li ion migration were performed at constant volume in supercells constructed from the optimized conventional cells extended by $1 \times 2 \times 2$. Molecular dynamics

calculations were performed with reduced planewave cutoff of $|\mathbf{k}+\mathbf{G}|^2 \leq 49$ bohr^{-2} and with a Brillouin-zone sampling grid of $1 \times 1 \times 1$. The simulations were performed for a microcanonical ensemble with a time integration step of $\Delta t = 0.48 \times 10^{-15}$ s. After an equilibration delay of approximately 0.1 ps, the temperature of the simulation was determined from the averaged kinetic energy of the ions.

III. Simulated crystal structures

There are two reported analyses of the crystal structure of Li_4SnS_4. [3, 4] The two analyses agree that the structure is characterized by the space group $Pnma$ (No. 62 in the International Table of Crystallography [21]), but differ slightly in the reported lattice constants and the fractional coordinates of one of the Li sites. [4] The structural analysis of MacNeil *et al.* [4] is perfectly ordered, while in the structural analysis of Kaib *et al.*, [3] the $4a$ Li sites are replaced by fractionally occupied $8d$ sites.

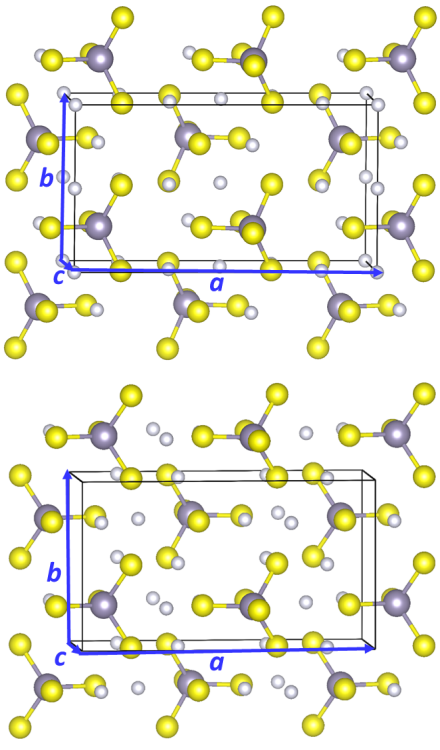

Figure 1: Ball and stick models of (a) Li_4SnS_4 and (b) $Li_4SnS_4^*$. Li, Sn, and S are represented by gray, purple, and yellow balls respectively.

TABLE I: Comparison of lattice parameters for Li_4SnS_4 and related compounds. Calculated parameters are scaled by factor of 1.02 to correct for systematic LDA error. Measured parameters are listed in parentheses.

	Li_4GeS_4	$Li_4GeS_4^*$
a (Å)	14.01 (14.06)[a]	13.49
b (Å)	7.74 (7.75)[a]	7.79
c (Å)	6.12 (6.15)[a]	6.30
E (eV/FU)	0.00	0.25
	Li_4SnS_4	$Li_4SnS_4^*$
a (Å)	14.25 (14.31)[a]	13.81 (13.81)[b]
b (Å)	7.86 (7.90)[a]	7.93 (7.96)[b]
c (Å)	6.31 (6.33)[a]	6.41 (6.37)[b]
E (eV/FU)	0.00	0.02
	Li_4SnSe_4	
a (Å)	(14.93)[c]	
b (Å)	(8.22)[c]	
c (Å)	(6.60)[c]	

[a]Ref. [4] [b]Ref. [3] [c]Ref. [22]

We computationally investigated both structures, finding that the ordered structure analyzed by MacNeil *et al.* [4] to be the ground state structure which we denote as "Li_4SnS_4". Simulations of ordered approximations to the disordered structure of Kaib *et al.* [3] find a meta-stable structure which we denote as "$Li_4SnS_4^*$" having an energy 0.02 eV/formula

unit higher in energy than the ground state structure. Ball and stick drawings of the two structures are shown in Fig. 1. The corresponding calculated and measured lattice constants are listed in Table I and the calculated and measured fractional coordinates are listed in Table II.

TABLE II: Comparison of fractional coordinates of unique atomic positions for Li_4SnS_4 and related compounds. The second column lists the site multiplicity and Wyckoff label. Measured parameters are listed in square brackets.

Atom	Site	Li_4GeS_4 (x, y, z)	$Li_4GeS_4^*$ (x, y, z)
Li	$4a$	$(0.000, 0.000, 0.000)$ $[(0.000, 0.000, 0.000)]^a$	–
Li	$4c$	–	$(0.260, 0.250, -0.001)$
Li	$4c$	$(0.412, 0.250, 0.127)$ $[(0.412, 0.250, 0.129)]^a$	$(0.429, 0.250, 0.216)$
Li	$8d$	$(0.177, 0.000, 0.186)$ $[(0.178, 0.000, 0.192)]^a$	$(0.147, -0.023, 0.139)$
Ge	$4c$	$(0.089, 0.250, 0.645)$ $[(0.089, 0.250, 0.649)]^a$	$(0.097, 0.250, 0.620)$
S	$4c$	$(0.084, 0.250, 0.277)$ $[(0.086, 0.250, 0.291)]^a$	$(0.105, 0.250, 0.261)$
S	$8d$	$(0.158, 0.010, 0.780)$ $[(0.157, 0.015, 0.779)]^a$	$(0.177, 0.019, 0.761)$
S	$4c$	$(0.437, 0.250, 0.728)$ $[(0.439, 0.250, 0.731)]^a$	$(0.434, 0.250, 0.810)$
Atom	Site	Li_4SnS_4 (x, y, z)	$Li_4SnS_4^*$ (x, y, z)
Li	$4a$	$(0.000, 0.000, 0.000)$ $[(0.000, 0.000, 0.000)]^a$	–
Li	$4c$	–	$(0.287, 0.250.0.003)$ $[-]^b$
Li	$4c$	$(0.410, 0.250, 0.124)$ $[(0.409, 0.250, 0.126)]^a$	$(0.429, 0.250, 0.359)$ $[(0.430, 250, 0.338)]^b$
Li	$8d$	$(0.176, 0.003, 0.178)$ $[(0.178, 0.004, 0.179)]^a$	$(0.158, -0.004, 0.149)$ $[(0.160, 0.005, 0.154)]^b$
Sn	$4c$	$(0.093, 0.250, 0.640)$ $[(0.092, 0.250, 0.642)]^a$	$(0.090, 0.250, 0.633)$ $[(0.087, 0.250, 0.635)]^b$
S	$4c$	$(0.080, 0.250, 0.255)$ $[(0.083, 0.250, 0.267)]^a$	$(0.092, 0.250, 0.256)$ $[(0.091, 0.250, 0.263)]^b$
S	$8d$	$(0.152, -0.005, 0.787)$ $[(0.161, 0.001, 0.784)]^a$	$(0.158, -0.004, 0.149)$ $[(0.167, 0.007, 0.767)]^b$
S	$4c$	$(0.430, 0.250, 0.732)$ $[(0.432, 0.250, 0.766)]^a$	$(0.423, 0.250, 0.748)$ $[(0.424, 0.250, 0.736)]^b$
Atom	Site	Li_4SnSe_4 (x, y, z)	$Li_4SnSe_4^*$ (x, y, z)
Li	$4a$	$[(0.000, 0.000, 0.000)]^c$	
Li	$4c$	$[(0.412, 0.250, 0.106)]^c$	
Li	$8d$	$[(0.178, 0.005, 0.180)]^c$	
Sn	$4c$	$[(0.092, 0.250, 0.643)]^c$	
Se	$4c$	$[(0.082, 0.250, 0.264)]^c$	
Se	$8d$	$[(0.161, -0.002, 0.784)]^c$	
Se	$4c$	$[(0.432, 0.250, 0.728)]^c$	

[a]Ref. [4] [b]Ref. [3] using coordinate shift of Ref. [4]; fractionally occupied Li positions are not listed. [c]Ref. [22]; coordinates shifted and rotated for consistency.

Interestingly, the main difference between the simulated structures of Li_4SnS_4 and $Li_4SnS_4^*$ is that four Li's per unit cell occupy different void regions between the SnS_4 tetrahedra. In the Li_4SnS_4 structure, the special Li ions occupy sites at the center and boundaries of the unit cell having multiplicity and Wyckoff label $4a$. In the $Li_4SnS_4^*$ structure, the special Li ions instead occupy sites interior to the unit cell having multiplicity and Wyckoff label $4c$. While the simulated fractional coordinates of the special Li ions for this $4c$ site

do not agree with the two $8d$ fractionally occupied coordinates found by Kaib *et al.*, [3] the optimized lattice constants are in excellent agreement, as shown in Table I.

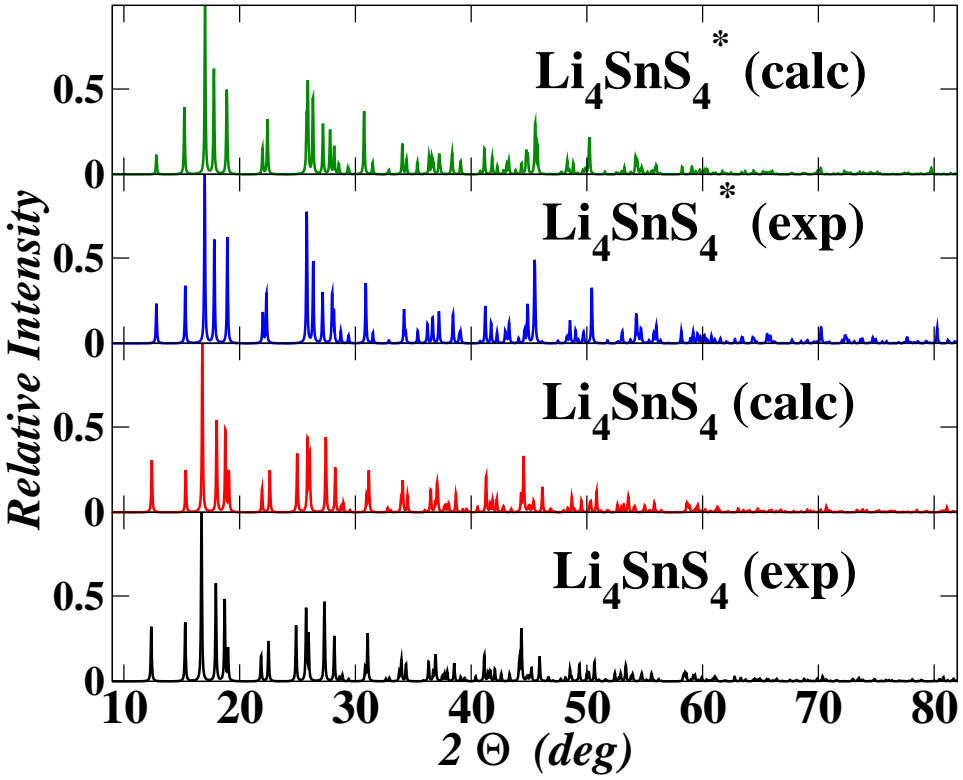

Figure 2: X-ray diffraction patterns generated by the Mercury software package [23] assuming an X-ray wavelength of $\lambda = 1.54056$ Å. The structural parameters from experiment were taken from Ref. [4] for Li_4SnS_4 and from Ref. [3] for $Li_4SnS_4^*$.

Because of its low atomic number, the X-ray signal for Li positions is notoriously small so that it is reasonable to ask whether the simulated $Li_4SnS_4^*$ structure might be compatible with the structural data reported by Kaib *et al.*, [3] even if the site analysis differs. Using the Mercury software package, [23] with the structural data from experiment and simulations we compare the computed X-ray patterns for the structures of Li_4SnS_4 and $Li_4SnS_4^*$ in Fig. 2. We see that the patterns for Li_4SnS_4 and $Li_4SnS_4^*$ are distinguishable and that there seems to be good agreement between our simulated structures and the corresponding X-ray results. While it would be better to compare the simulated diffraction patterns directly with the experimental data, the good agreement between the simulations and the fitted results from experiment shown in Fig. 2 is encouraging. It is interesting to note that two other groups [5, 6] have recently reported preparation of Li_4SnS_4 using relatively low temperature processing similar to that of Kaib *et al.* [3] and their reported X-ray diffraction diffraction patterns show strong similarity to the patterns for $Li_4SnS_4^*$ shown in Fig. 2. Presumably, the ground state Li_4SnS_4 structure is accessible using the higher temperature processes described in Ref. [4].

It is also interesting to note that Kaib *et al.* [22] also recently synthesized Li_4SnSe_4 using relatively high temperature techniques, finding it to take the "ground state" structure as listed in Table I and in Table II. We have not yet performed computer simulations on the selenide material. On the other hand, we did ask the question whether the structurally and chemically similar material Li_4GeS_4 behaves in a similar way. The results for the the Li_4GeS_4 and $Li_4GeS_4^*$ structures are listed in Table I and in Table II. The structural pattern is very similar to that of Li_4SnS_4. However, in this case, we would predict that the $Li_4GeS_4^*$ structure is less likely to form since its energy is predicted to be 0.25 eV/formula unit higher in energy than the ground state energy.

III. Partial Densities of States

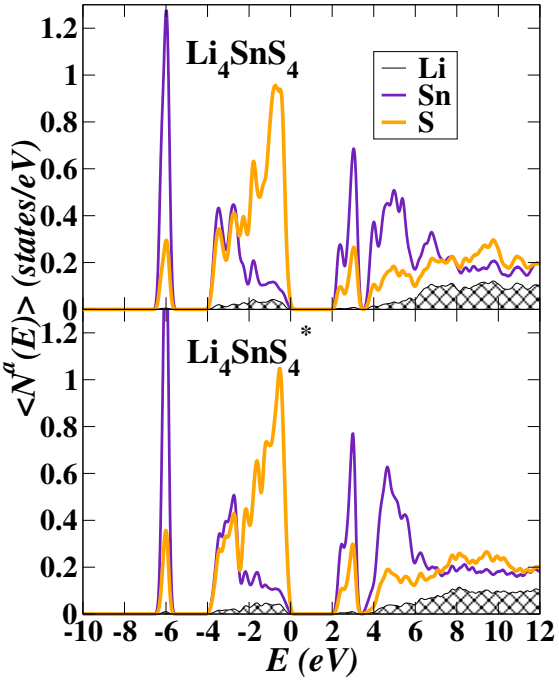

Figure 3: Partial densities of states for Li_4SnS_4 and $Li_4SnS_4^*$, separately indicating contributions from Li, Sn, and S sites.

In order to gain a qualitative understanding of the electronic structure of the various forms of Li_4SnS_4, it is helpful to analyze the partial densities of states which are shown in Fig. 3. The two structures have nearly indistinguishable partial density of states curves. The material is clearly an insulator with a band gap expected to be larger than 2 eV found in the present study due to the systematic gap underestimation known for LDA calculations.

IV. Mechanisms for Li Ion Migration

In studying the ion migration mechanisms for the Li_4SnS_4 and $Li_4SnS_4^*$ structures, we find the Li ion motions to be highly correlated presumably due to a complicated energy

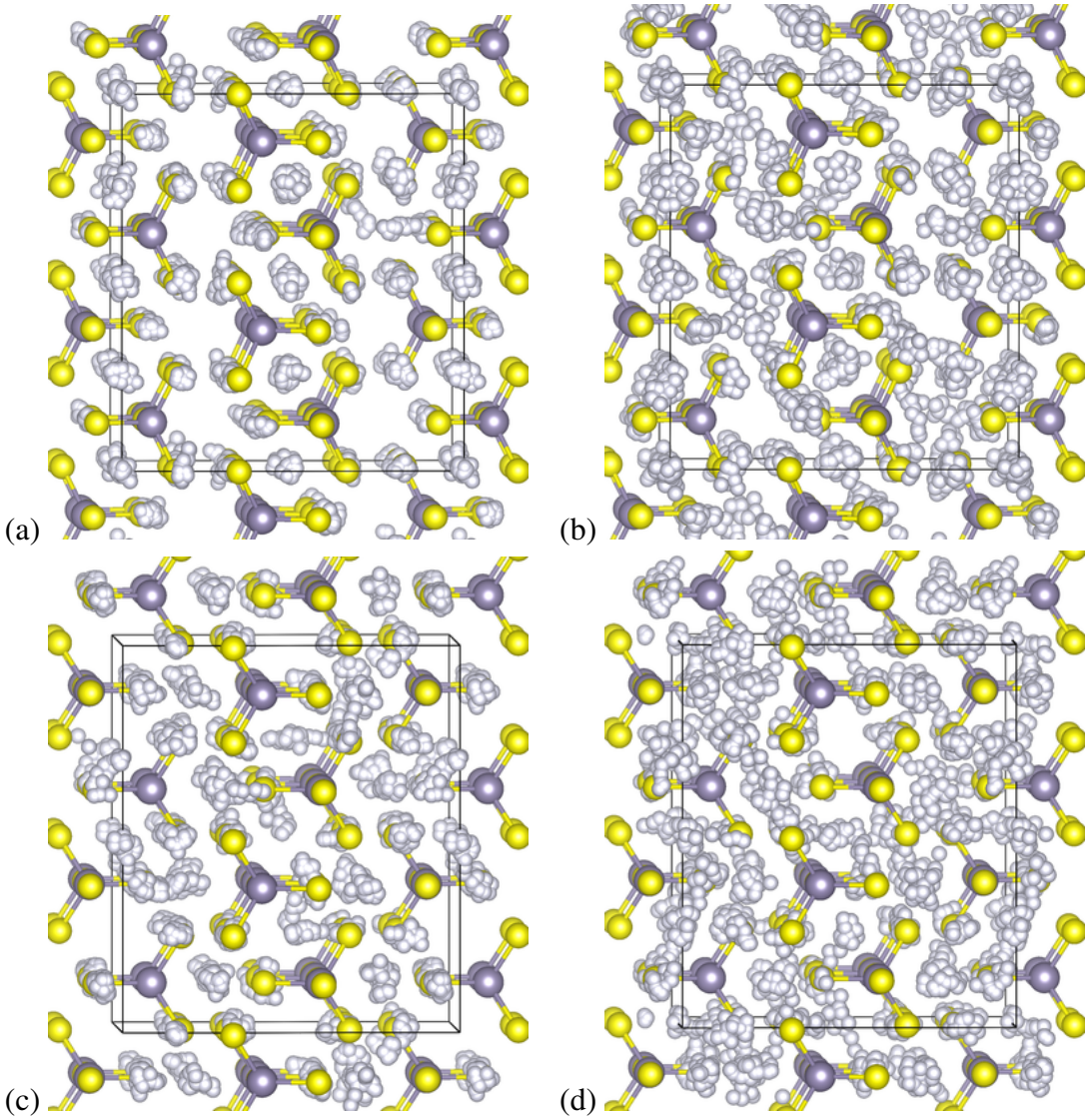

Figure 4: Ball and stick diagrams of molecular dynamics simulations for (a) Li_4SnS_4 at T= 582 K, (b) Li_4SnS_4 at T= 1112 K, (c) $Li_4SnS_4^*$ at T= 571 K, and (d) $Li_4SnS_4^*$ at T= 1106 K. Initial Sn and S positions are represented by purple and yellow balls respectively. Li positions of initial configuration and subsequent positions at intervals of 0.024 ps are indicated with gray balls. Simulations were performed using microcanonical ensembles (constant energy and volume) in $1 \times 2 \times 2$ supercells, oriented as in Fig. 1.

landscape. In both structures, some of the vacancy sites are unstable. For example, in the Li_4SnS_4 structure, a d site vacancy is unstable relative to a vacancy on the nearest special $4a$ site Li. In the $Li_4SnS_4^*$ structure a d site vacancy is unstable relative to a vacancy on the nearest special $4c$ site Li. In order to get a qualitative picture of the migration processes, we performed molecular dynamics simulations using the QUANTUM ESPRESSO [11] code for two different microcanonical ensembles for each material. Ball and stick models of the crystals with superposed Li positions at 30 time steps at intervals of 0.024 ps are shown in Fig. 4. Comparing the simulated Li ion trajectories in the two structures at low temperature ($T \approx 600$ K), it is evident that the Li ions in the $Li_4SnS_4^*$ structure have greater range than they do in the Li_4SnS_4 structure. Further investigation shows that the c-axis migration is favored in the Li_4SnS_4 structure, while the migration is more isotropic in the $Li_4SnS_4^*$ structure.

Unfortunately, the simulations we have carried out so far are insufficient for quantitative estimates, although we can make the following very preliminary analysis, following the approach pioneered by Ong *et al.* [24, 25, 26] For a molecular dynamics simulation at temperature T with resultant ion trajectories $\{\mathbf{r}_i(t)\}$ as a function of time t, one can calculate the mean squared displacement and use Einstein's expression for the diffusion constant at that temperature $D(T)$: [27]

$$\left\langle \frac{1}{6N} \sum_{i=1}^{N} |\mathbf{r}_i(t) - \mathbf{r}_i(t_0)|^2 \right\rangle = D(T)[t - t_0] + C. \tag{1}$$

Here the summation over i denotes the N Li ion positions $\{\mathbf{r}_i(t)\}$ in the simulation cell and C denotes a constant. In order to improve the sampling of the simulation, the incremental distance is averaged over the initial times t_0 as implied by the angular brackets in the expression. Since diffusion takes place near equilibrium, it is reasonable to also assume that the diffusion coefficient has an Arrhenius temperature dependence [28]

$$D(T) = D(0)\mathrm{e}^{-E_A/kT}, \tag{2}$$

where $D(0)$ denotes the diffusion coefficient at 0 K, E_A denotes the activation energy for diffusion, and k denotes the Boltzmann constant. From the simulations we estimate that $E_A = 0.3 \pm 0.1$eV and $E_A = 0.2 \pm 0.1$ eV for Li_4SnS_4 and $Li_2SnS_4^*$ eV respectively. These estimates are significantly smaller than the experimental values which find $E_A = 0.4$ eV [3, 6] for $Li_2SnS_4^*$. While the values of E_A simulated in this way are smaller than expected the trend that $E_A[Li_4SnS_4] > E_A[Li_4SnS_4^*]$ is reasonable. To further relate these results to ionic conductivity, we can use the Nernst-Einstein relation

$$\sigma(T) = D(0) f_{NE} \frac{\rho q^2}{kT} \mathrm{e}^{-E_A/kT}, \tag{3}$$

where ρ denotes the number of mobile ions per unit volume, q denotes the charge of each mobile ion, and f_{NE} is the Nernst-Einstein factor. [29] In order to make an order of magnitude estimate of the conductivity of the present system, we can approximate $f_{NE} = 1$, although we expect it to deviate significantly for our strongly correlated material. The resulting estimates of the ionic conductivity for our simulated materials are a few orders of

magnitude too high – $\sigma_{300K}[Li_4SnS_4] \approx 3$ mS/cm and $\sigma_{300K}[Li_4SnS_4^*] \approx 80$ mS/cm. However, the result that the conductivity of the $Li_4SnS_4^*$ form is greater than that of the ground state structure is expected.

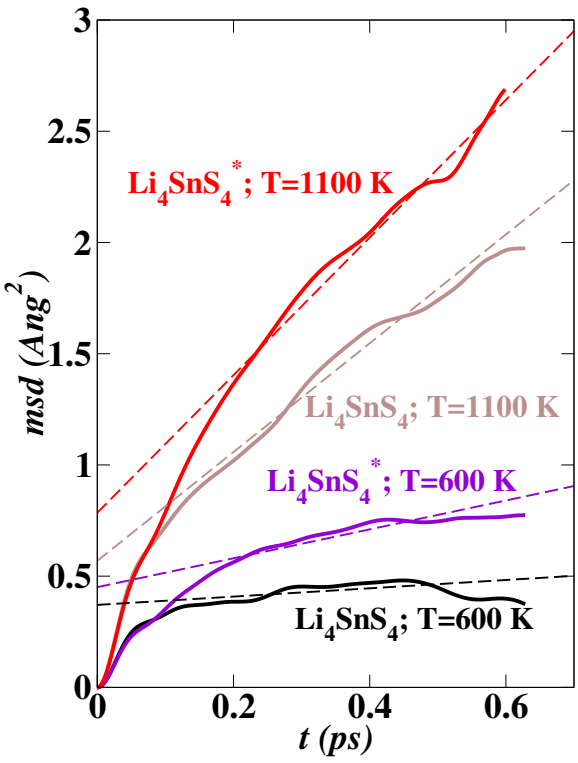

Figure 5: Plot of mean squared displacement data (msd) in units of Å^2 versus time interval in units of pico seconds for $1 \times 2 \times 2$ supercells of Li_4SnS_4 and $Li_4SnS_4^*$ structures at temperatures 600 K and 1100K as indicated. Straight lines show linear fits according to Eq. (1).

V. Summary and Conclusions

The preliminary simulation results reported here support the experimental findings that Li_4SnS_4 is a promising Li ion electrolyte, particularly in its meta-stable $Li_4SnS_4^*$ structural form. The experimental reports [3, 4, 5, 6] suggest that the ground state structure is obtained by high temperature (750° C) synthesis while the meta-stable structure is obtained at lower temperature. Our simulations of the two structures show that the most energetically favorable interstitial position for Li ions in the Li_4SnS_4 structure are occupied sites in the $Li_4SnS_4^*$ structure and vice versa. In our simulations, the $Li_4SnS_4^*$ structure is ordered and differs somewhat from the analysis of Kaib *et al.*, [3] but is consistent with the reported X-ray pattern.

Our first principles molecular dynamics simulations are too preliminary to give quantitative predictions, but suggest that the $Li_4SnS_4^*$ structure supports isotropic Li ion migration, while Li ion migration in the ground state structure favors c-axis migration.

Acknowledgments

This work was supported by NSF grant DMR-1507942. Computations were performed on the Wake Forest University DEAC cluster, a centrally managed resource with support provided in part by the University. Helpful discussions with Jennifer A. Aitken from Duquesne University, Joseph H. MacNeil from Chatham University, and Larry E. Rush, Jr., Jason Howard, and Ahmad Al-Qawasmeh from Wake Forest University are gratefully acknowledged.

References

[1] Y. Wang, *et al.*, *Nature Materials* **14**, 1026 (2015).

[2] J. Li, C. Ma, M. Chi, C. Liang, N. J. Dudney, *Advanced Energy Materials* **5**, 1401408 (2015).

[3] T. Kaib, *et al.*, *Chemistry of Materials* **24**, 2211 (2012).

[4] J. H. MacNeil, *et al.*, *Journal of Alloys and Compounds* (2013).

[5] G. Sahu, *et al.*, *Energy Environ. Sci.* **7**, 1053 (2014).

[6] K. H. Park, *et al.*, *Advanced Materials* **28**, 1874 (2016).

[7] P. Hohenberg, W. Kohn, *Physical Review* **136**, B864 (1964).

[8] W. Kohn, L. J. Sham, *Physical Review* **140**, A1133 (1965).

[9] P. E. Blöchl, *Phys. Rev. B* **50**, 17953 (1994).

[10] N. A. W. Holzwarth, A. R. Tackett, G. E. Matthews, *Computer Physics Communications* **135**, 329 (2001). Available from the website `http://pwpaw.wfu.edu`.

[11] P. Giannozzi, *et al.*, *J. Phys.: Condens. Matter* **21**, 394402 (19pp) (2009). Available from the website `http://www.quantum-espresso.org`.

[12] X. Gonze, *et al.*, *Computer Physics Communications* **180**, 2582 (2009). Code is available at the website `http://www.abinit.org`.

[13] A. Kokalj, *Journal of Molecular Graphics and Modelling* **17**, 176 (1999). Code available at the website `http://www.xcrysden.org`.

[14] A. Kokalj, *Computational Materials Science* **28**, 155 (2003).

[15] K. Momma, F. Izumi, *Applied Crystallography* **44**, 1272 (2011). Code available from the website `http://jp-minerals.org/vesta/en/`.

[16] J. P. Perdew, Y. Wang, *Phys. Rev. B* **45**, 13244 (1992).

[17] Y. A. Du, N. A. W. Holzwarth, *Phys. Rev. B* **76**, 174302 (14 pp) (2007).

[18] Y. A. Du, N. A. W. Holzwarth, *Phys. Rev. B* **81**, 184106 (15pp) (2010).

[19] Z. D. Hood, *et al.*, *Solid State Ionics* **284**, 61 (2015).

[20] N. D. Lepley, N. A. W. Holzwarth, Y. A. Du, *Phys. Rev. B* **88**, 104103 (11 pp) (2013).

[21] T. Hahn, ed., *International Tables for Crystallography, Volume A: Space-group symmetry, Fifth revised edition* (Kluwer, 2002). ISBN 0-7923-6590-9. The symmetry labels used in this work are all based on this reference.

[22] T. Kaib, *et al.*, *Chemistry of Materials* **25**, 2961 (2013).

[23] Mercury 3.5.1 (2014). Developed and distributed by the Cambridge Crystallographic Data Centre `http://www.ccdc.cam.ac.uk/mercury/`.

[24] S. P. Ong, O. Andreussi, Y. Wu, N. Marzari, G. Ceder, *Chemistry of Materials* **23**, 2979 (2011).

[25] Y. Mo, S. P. Ong, G. Ceder, *Chemistry of Materials* **24**, 15 (2012).

[26] Z. Zhu, I.-H. Chu, Z. Deng, S. P. Ong, *Chemistry of Materials* **27**, 8318 (2015).

[27] J. M. Haile, *Molecular Dynamics Simulations* (John Wiley & Sons, Inc., 1992).

[28] J. Maier, *Physical Chemistry of Ionic Materials* (John Wiley and Sons, Ltd., 2004).

[29] B. J. Morgan, P. A. Madden, *Physical Review Letters* **112** (2014).